Ruthenium Volatilisation from Reprocessed Spent Nuclear Fuel – Studying the Baseline Thermodynamics of Ru(III)

Sukhraaj K. Johal[a], Colin Boxall[a]*, Colin Gregson[b],Carl J. Steele[c]

[a]The Lloyd's Register Foundation Centre for Nuclear Engineering, Engineering Department, Lancaster University, Bailrigg, Lancashire, LA1 4YR, U.K.
[b]National Nuclear Laboratory, Sellafield, Seascale, Cumbria, CA20 1PG, U.K.
[c]Sellafield Ltd., Sellafield, Seascale, Cumbria, CA20 1PG, U.K.

Ruthenium is a fission product possessed of two relatively long lived isotopes, ^{103}Ru and ^{106}Ru, both of which form part of the Highly Active (HA) waste raffinate during spent nuclear fuel reprocessing. During reprocessing ruthenium, which may be in the form of the $RuNO^{3+}$ complex, encounters temperatures conducive to volatilization. Due rutheium's high specific radioactivity it is important to understand the mechanism by which volatilisation occurs. Here we use combined CV, RDE and electrochemical microgravimetry experiments in a study of the the $RuCl_3$ system for the first time. We do this in the interest of establishing NO-free Ru(III) baseline behaviour so as to support future studies on NO complexed ruthenium. Using wide aqueous solvent window carbon electrodes we have observed discrete oxidations to a solution phase Ru(III)–Ru(IV)–Ru(III) trimer, to solid RuO_2 and volatile RuO_4. We have also observed and assigned discrete reductions of solid RuO_2 back to Ru(III) and Ru(III) reduction to ruthenium metal.

Introduction

Spent nuclear fuel management at the UK's Sellafield reprocessing plants includes the reprocessing of spent nuclear fuel by the solvent extraction-based PUREX (Plutonium Uranium Redox EXtraction) process. This produces a Highly Active (HA) waste aqueous raffinate which is concentrated into evaporators and storage tanks in the Highly Active Liqour Evaporation and Storage (HALES) facility. From there, it is fed to the Waste Vitrification Plant (WVP) where the resultant Highly Active Liquor (HAL) feed is calcined and combined with glass to produce an immobilised HA waste form.

Ruthenium is a fission product with 2 relatively long lived isotopes; ^{103}Ru and ^{106}Ru, $t_{1/2}$ = 39.8 days and 1 year respectively, both isotopes form part of the wider inventory of fission products within the HA raffinate. Volatilisation of fission products in nuclear waste generally occurs at high temperature – apart from ruthenium where volatilisation occurs at the lower temperature stages of the three stage vitrification process. These are:

1. The HAL is evaporated to dryness
2. The solid residues are calcined (denitration to the oxides occurs in this stage)
3. The calcined oxides are fused into a glass melt.

Volatile Ru generation mainly occurs as the last of the liquid is removed and the material becomes a solid. Dust and other volatiles are removed from the vessel ventilation system via a dust scrubber, condenser and NOx absorber (primary off-gas system) followed by an electrostatic precipitator (ESP), wet scrubber and two banks of HEPA filters

(secondary off-gas system) to avoid release of radioactive isotopes (including ^{106}Ru and ^{103}Ru) to the environment via the WVP stack. However, given its volatile nature and high specific radioactivity ruthenium presents a strong challenge to the nuclear industry in effectively managing its abatement. Especially, vitrification at Sellafield has been scrutinised since the discharge of 3.1 GBq of volatile ^{106}Ru via the WVP in 1997. Thus, understanding the highly complex solution chemistry of ruthenium is essential as it is widely believed a redox state change from Ru (III) to Ru (VIII) is responsible for volatilisation of ruthenium via RuO_4 formation. (1-8)

Nitrite and nitrous acid are produced within the HAL by radiolysis of the concentrated nitric acid used in the PUREX aqueous process streams and thus the HA raffinate. However, neither is stable in acid solution, decomposing to form NO and NO_2 via N_2O_3. NO in particular forms a strong affiliation with Ru(III) (9) resulting in the formation of the nitrosyl ruthenium [$Ru(NO)^{3+}$] species that is ubiquitous in HAL chemistry.

The chemical mechanism of ruthenium changing from a solution species either as free Ru^{3+} or $Ru(NO)^{3+}$, to a volatile form is poorly understood. Current assumptions (10) are that, in nitric acid media, ruthenium nitrosyl nitrates [$Ru(NO)(NO_3)_x(H_2O)_{5-x}$] where x = 3,4 are the most likely candidates to oxidise to volatile ruthenium, considered to be RuO_4 (*vide supra*). It is reported that in excess of 70% of ruthenium in solution can exist as [$Ru(NO)(NO_3)_{3-4}(H_2O)_{1-2}$] at high acidity. Furthermore, recent experimental work within the UK National Nuclear Laboratory (5) has demonstrated that the presence of oxidising metal ions in HA waste (e.g. Ce(IV)) can enhance the volatility of ruthenium through a chemical conversion of Ru(III) species to what is, again, assumed to be RuO_4. Therefore, a better understanding of these species, their electrochemical processes and reaction kinetics is required to underpin the empirical evidence gathered to date.

Several studies have investigated the redox state changes of ruthenium in acid media, both in the presence and absence of nitrate. These are summarized in Table 1 and described as follows. Wehner and Hindman (11) investigated electrolytic preparation methods of Ru (III) and Ru (IV) and subsequent absorption spectra. They studied the electrochemical transition of the Ru (III) to Ru (IV) redox couple from a solution of Ru (IV) in various concentrations of $HClO_4$ prepared from the electrolytic reduction of RuO_4 solutions. They reported the formal potential of Ru (III) to Ru (IV) to lie in a range between 0.55 and 1.17 V vs the normal hydrogen electrode (SCE). Consistent with this range, polarographic studies of the Ru (III) to Ru (IV) transition by Niedrach and Tevebaugh (12) quoted a value of 0.65 V vs. NHE for the standard electrode potential of Ru (III) to Ru (IV) in $HClO_4$. This value was also in agreement with that obtained by Atwood and DeVries (13) from a polarography study of the reduction of Ru (IV) in $HClO_4$, in which they obtained a value of 0.59 V vs. NHE.

More recently, Maya (14) studied the reduction of Ru (IV), prepared from the photolytic dissociation of ruthenium nitrosyl nitrate solutions to Ru(III) solutions, these were allowed to spontaneously oxidise up to Ru(IV). These were in the form of $Ru_4(OH)_{12}^{4+}$) in a $HNO_3/NaNO_3$ mixture and Maya reported reduction peaks at 0.15, 0.35, 0.92 V vs. saturated calomel electrode (SCE) which they attribute to tetramer chemistry. These features were also observed by Wallace and Propst (15) and were within 10 mV of the values reported by Maya. It was found each process involved a 1 e^- transfer corresponding to the reduction of Ru (IV) species to species with average oxidation states of 3.75 & 3.5 at the potentials of 0.35 & 0.15 V respectively. In a study of Ru(IV) containing solutions, Wehner and Hindman (11) observed reactions at 0.96 and 1.16 V vs SCE on platinum, attributing the latter irreversible oxidation at 1.16 V to formation of RuO_4 from Ru(IV) and the process at 0.96 V to formation of a species with an average

Table 1: Summary of formal potentials reported in the literature for key Ru redox transitions between the Ru(III) and Ru(VIII) oxidation states. All potentials reported have been rescaled with reference to the SCE.

Potential / V vs SCE	Assigned Process	Expt Details	Authors	Ref No
0.31-0.93	Ru(III)/Ru(IV) n=1	Oxidation on Pt in $HClO_4$ at pH 0	Wehner & Hindman	(11)
0.41	Ru(III)/Ru(IV) n=1	Oxidation on Pt in $HClO_4$ at pH 0	Niedrach & Tevebaugh	(12)
0.35	Ru(III)/Ru(IV) n=1	Reduction on Pt in $HClO_4$ at pH 1	Atwood & DeVries	(13)
0.15	Ru(3.5)/Ru(IV) n=0.5	Reduction on Pt in 0.9M $NaNO_3$ and 0.1M HNO_3	Maya	(14)
0.35	Ru(3.75)/Ru(IV) n=0.25	Reduction on Pt in 0.9M $NaNO_3$ and 0.1M HNO_3	Maya	(14)
0.92	Ru(IV)/Ru(4.38) n=0.38	Reduction on Pt in 0.9M $NaNO_3$ and 0.1M HNO_3	Maya	(14)
0.96	Formation of Ru(4.38) from Ru(IV)	Oxidation on Pt in $HClO_4$ at pH 0	Wehner & Hindman	(11)
1.16	Formation of Ru(VIII) from Ru(IV)	Irreversible oxidation on Pt in $HClO_4$ at pH 0	Wehner & Hindman	(11)
0.395	Ru(IV)/Ru(3.75)	Reduction on Au in HNO_3 at pH -0.5	Mousset	(10)
0.895	Ru(IV)/Ru(4.38)	Reduction on Au in HNO_3 at pH -0.5	Mousset	(10)
1.095	Ru(III)/Ru(VIII)	Oxidation on Au in HNO_3 at pH 3	Mousset	(10)
1.495	Ru(III)/Ru(VIII)	Oxidation on Au in HNO_3 at pH 3	Mousset	(10)

oxidation state of 4.38. Mousset (10) studied electrovolatilisation from $RuO_2.xH_2O$ and commercial $RuNO^{3+}$ solutions. $RuO_2.xH_2O$ showed reduction processes at ~0.4 and 0.9 V vs Ag/AgCl, in good agreement with Maya's (14) reported reduction potentials. Mousset's electrovolatilisation studies on $RuNO^{3+}$ solutions indicated oxidation processes at 1.1 and 1.5 V vs Ag/AgCl attributed to RuO_4 generation reactions.

However, the data summarized in Table 1 has several issues with regards to the oxidation behaviour of Ru(III). Notwithstanding the lack of consensus regarding peak assignment, especially those relating to higher oxidation state transitions, much of the data relates to the reduction of solution phase Ru(IV), with the oxidation behaviour of the generated reduction product being indirectly inferred; this is complicated by that product rarely being monomeric Ru(III) but rather Ru(III)-Ru(IV) oligomers (*vide supra*).

Additionally, a number of the studies cited are conducted using Au or Pt electrodes, systems that have two limitations with respect to study of the Ru(III) system: (i) oxygen evolution as a result of water oxidation on Au or Pt occurring at ~0.99 V vs. SCE at pH 0, potentially masking higher potential oxidation reactions of Ru such as Ru(IV) to Ru(VIII) under conditions relevant to HAL chemistry, see figure 1 (16); and (ii) especially for gold, the assignment of peaks observed in the cyclic voltammetry of Ru(III)/Ru(IV) solutions

at lower potentials than oxygen evolution being complicated by the intrinsic electrochemistry of electrode itself. The latter includes gold oxide formation and stripping peaks which occur in the range +1.24 to +1.41 V and 0.55 to 0.75 V vs SCE respectively, and the oxidation and reduction of so-called Burke sites (a sub-monolayer of low coordination state Au atoms at the gold electrode surface (17-19) which occur in the range 0.4 to 0.6 V vs SCE at pH 0 (20) and so overlap, and may be confused with, many of the monomeric and oligomeric Ru(III)/Ru(IV) in this range (see Table 1).

Unfortunately, extant thermodynamic data related to Ru redox chemistry are not helpful here. Fig 1&2 show both the Ru-H_2O E_h-pH (Pourbaix) diagram (16) and Ru Latimer diagram (21), neither of which report on data related to Ru(III)/Ru(IV) redox couple where Ru(III) is present in the solution phase. Indeed, the Latimer diagram provides no data on the Ru(IV)/Ru(III) transition at all.

Given these uncertainties, this paper presents a study of the behaviour of NO-free Ru(III) in order to underpin studies of NO complexed ruthenium, to be presented in a subsequent communication. Particularly, we study the oxidation reactions of Ru(III) species at acidities relevant to HAL, seeking to characterize key redox transitions (redox potentials, number of electrons transferred) and properties of electroactive species (diffusion coefficients). The initial studies presented here focus on the obtaining of values for these parameters by standard electrochemical methods (cyclic voltammetry, rotating ring-disc electrode) using readily available $RuCl_3$ samples and electrode materials such as glassy carbon possessed of little intrinsic electrochemistry (in contrast to the gold electrode based studies of Table 1) and wide solvent windows so facilitating the study of redox couples with highly anodic E^{θ} values. Coupled electrochemical / microgravimetric measurements are used to obtain a more robust view of what is occurring during the redox processes understudy, especially in terms of solid phase formation and loss.

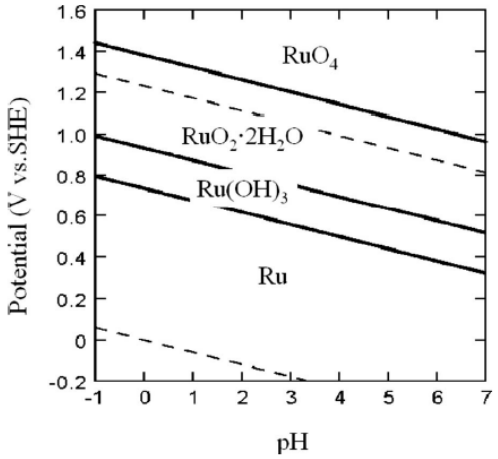

Figure 1 – Eh-pH (Pourbaix) diagram for the Ru-H_2O system (taken from ref. 16)

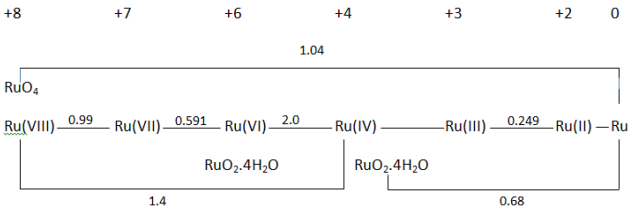

Figure 2 – Ru Latimer diagram at pH 0

Experimental

Materials and reagents

All reagents were ACS reagent grade or higher and purchased from Fisher Scientific (Loughborough, UK) or Sigma Aldrich (Gillingham, Dorset, UK) and used without further purification. Doubly distilled water, further purified by a deionisation system (E-pure model 04642, Barnstead/Thermodyne, Dubuque, IA, USA) to a resistivity of 1.8 x 10^5 Ωm. Nitrogen (99.998% grade) was supplied by BOC Ltd. (Guilford, Surrey, UK).

$RuCl_3.xH_2O$ solution preparation

Solutions of $RuCl_3.xH_2O$ (10 mol dm^{-3}) were made in $HClO_4$ (0.1 mol dm^{-3}) made up with distilled water. Prior to electrochemical analysis, all solutions were purged with N_2 for 20 minutes to remove dissolved O_2.

Exhaustive electrolysis

Electroreduction of as prepared $RuCl_3$ solutions, via exhaustive electrolysis, was carried out in a separated cell using an agar/ $KClO_4$ salt bridge, made with distilled water, under an inert N_2 atmosphere. The solution was left stirring for 12 hours at 0.2 V. Pt wire mesh was used as a working electrode (Goodfellow Cambridge Ltd., Huntingdon, UK.)

Electrochemical measurements

All electrochemical measurements, unless otherwise stated, were made using a freshly polished glassy carbon (2.9 mm diameter) working electrode in a 3 electrode cell with a Pt wire mesh (Goodfellow Cambridge Ltd., Huntingdon, UK) counter electrode and a Ag/AgCl (Alvatek Ltd. Tetbury, Gloucestershire, UK) reference electrode used in a double junction (Alvatek Ltd. Tetbury, Gloucestershire, UK) configuration with saturated K_2SO_4 solution. The working electrode was polished using decreasing grades of diamond slurries (6, 3, 1 μm) (Macron) with a final polish on a clean polishing pad soaked in distilled water. After polishing, the electrode was sonicated for 30s at 20W power in ethanol then distilled water to remove any debris remaining from polishing stages. All measurements were conducted at room temperature and under an inert N_2 atmosphere.

Rotating disk electrode (RDE) studies were carried out with a glassy carbon (7.2 mm diameter) working electrode and were not carried out under an inert N_2 atmosphere.

Electrochemical microgravimetric measurements

The electrochemical quartz crystal microbalance (EQCM) is a well-established method for the measurement of small changes in electrode mass due to reactions occurring at the electrode-solution interface. A detailed description of QCM theory may be found in various texts (21-24). Assuming mass is rigidly bound; the measured shift in the resonant frequency is converted to a mass change via the Sauerbrey equation, Equation [1]

$$\Delta f = -C_f \Delta m \qquad [1]$$

Where Δf is the change in resonant frequency (Hz), Δm is the mass change (g) and C_f is the sensitivity constant. The value of C_f can be determined from electrochemical deposition and dissolution of copper via cyclic voltammetry (25, 26) we have found it to be 0.059 Hz (ng cm^{-2}), which is in excellent agreement with a theoretical value of 0.056 Hz (ng cm^{-2}) quoted by the manufacturer (Q-sense, Biolin Scientific, Manchester, UK).

EQCM experiments used quartz crystals (SciMed Ltd., Stockport, Cheshire, UK) coated with amorphous carbon, 14 mm diameter, AT cut with a 10 MHz resonant frequency. Experiments were performed in a ground floor lab sited directly on building foundations and isolated from heavy machinery and vibration sources.

Analysis

All electrochemical measurements, unless otherwise stated, were made using an Autolab potentiostat PGSTAT128N equipped with a low current amplifier (Metrohm UK Ltd., Runcorn, Cheshire, UK). EQCM experiments were collected using a Gamry Potentiostat model 600, coupled with a Gamry EQCM model 10M (SciMed Ltd., Stockport, Cheshire, UK) allowing simultaneous QCM and potentiometric measurements to be taken.

Ultraviolet visible (UV-vis) spectroscopy was carried out with a Gamry spectro-115 spectrometer (SciMed Ltd., Stockport, Cheshire, UK) with a 1 cm path length quartz cuvette. All measurements, unless otherwise stated, were conducted in 0.1 mol dm^{-3} $HClO_4$ and spectra were referenced to a 0.1 mol dm^{-3} $HClO_4$ solution.

Results and Discussion

In order to provide a direct comparison between the work presented with that in the literature (see Table 1), Ru(III) electrochemistry was first studied by running a cyclic voltammogram (CV) of a solution of as-received $RuCl_3$ in $HClO_4$ using a 250 μm diameter gold microdisc as working electrode. Fig. 3 shows a full CV recorded over the range -1 to +2 V vs Ag/AgCl as well as an expanded scale inset showing the features in the range -0.15 to 0.8V. The oxidation peak at 1.1 V is co-incident with gold oxide formation at pH 1 (20), while the Ru-H_2O E_h-pH diagram and Latimer diagram of Fig. 1 & 2 indicate that it may have a significant component associated with Ru(VIII) evolution.

The inset of Fig.3 shows a reduction peak at ~0.7 V which we assign to an interfering gold oxide stripping (20). It also reveals the presence of apparently reversible processes at 0.25 and 0.4V. These are in close accordance, both in appearance and position, with

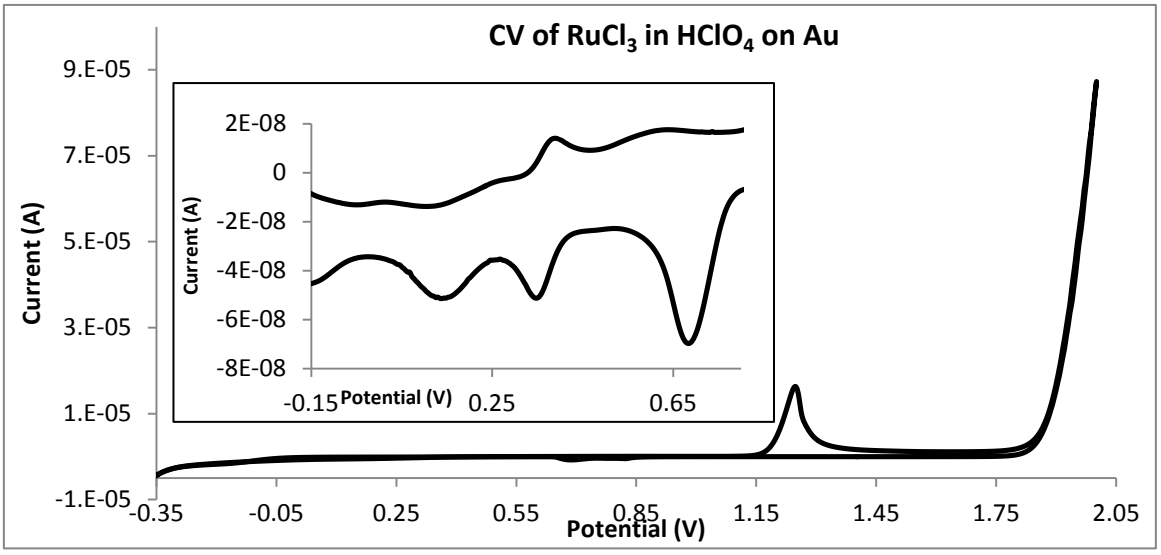

Figure 3 – CV of 10 mol $dm^{-3}RuCl_3$ in 0.1 mol $dm^{-3}HClO_4$ using a Au working electrode (250 μm diameter), Scan rate: 0.1 V s^{-1}. Inset: expanded scale from -0.15 to 0.8V

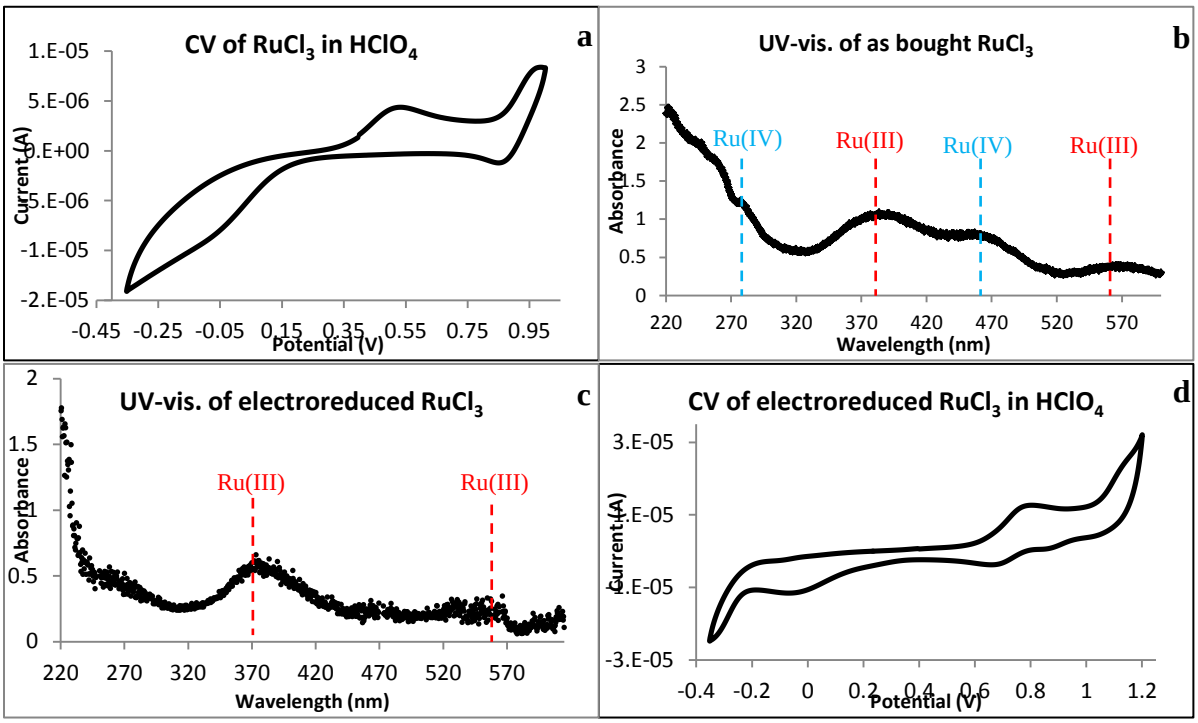

Figure 4 - a) CV of $RuCl_3$ (10 mol dm^{-3}) in $HClO_4$ (0.1 mol dm^{-3}) Scan rate: 0.1 Vs^{-1}, b) UV-vis. spectrum of as bought $RuCl_3$ (100 mol dm^{-3}) in $HClO_4$ (0.1 mol dm^{-3}), c) UV-vis. spectrum of electroreduced $RuCl_3$ (100 mol dm^{-3}) in $HClO_4$ (0.1 mol dm^{-3}) d) CV of electroreduced $RuCl_3$ (10 mol dm^{-3}) in $HClO_4$ (0.1 mol dm^{-3}). Scan rate: 0.1 V s^{-1},

voltammetric features recorded by Maya (12) who reported reversible peaks at 0.15 and 0.35 V during a study of the reduction of Ru(IV) solutions using a platinum working electrode. Maya assigned these to reactions involving Ru oligomers in the following average oxidation states: Ru(3.5)/Ru(3.75) at 0.15 V; and Ru (3.75)/Ru(IV) at 0.35 V, an assignment we therefore adopt for our peaks at 0.25 and 0.4 V. This leads to the curious conclusions that (i) solutions of as received $RuCl_3$ exhibit no oxidation features attributable to free /monomeric Ru(III); and (ii) the voltammetry is dominated by Ru(III)-Ru(IV) oligomer electrochemistry – despite, nominally, there being no Ru(IV) initially present in the $RuCl_3$ solution under study.

In order to eliminate any potential interferences from gold electrochemistry, the experiment of Fig.1 was repeated using a glassy carbon disc as working electrode, the resulting CV being shown in Fig. 4a. The observed voltammetric features are much more clearly resolved than in Fig. 3 with two peaks clearly visible at 0.55 and 0.9 V. Maya also reported a peak at 0.9 V which they attribute to tetramer oxidation, Ru(IV) to (4.38). Given this result, and the apparent presence in the voltammetry of as-received $RuCl_3$ solutions of Ru(IV) species (Fig.3), the (nominally) $RuCl_3$ solutions used in Figs. 3 & 4a were analysed using UV-vis. spectroscopy, Fig. 2b, in order to identify Ru species initially present. Wehner & Hindman (9) and Yan *et al* (27) report that absorption bands for $RuCl_3$ appear at 400 and 525nm and for Ru(IV) at 475 and 310nm. All four bands are present in the UV-vis spectrum of Fig. 4b, confirming that a mixture of Ru in +3 and +4 oxidation states is present in solutions prepared from as-prepared $RuCl_3$ – indicating the Ru(III) species in this form has a high susceptibility towards aerial oxidation.

Thus, a 12 hour exhaustive electroreduction treatment at 0.2V (see experimental section above) was used to generate Ru(IV)-free $RuCl_3$ solutions. Fig. 4c shows a UV-vis. spectrum of a post-treatment $RuCl_3$ solution, confirming the loss of the Ru(IV) absorption bands at 475 nm and 310 nm. Fig. 4d shows the CV of the resultant solution from which it can be seen that the peak observed at 0.55 V in Fig. 4a has disappeared suggesting it was associated with the oxidation of Ru(IV) species or Ru(IV) containing oligomers. In contrast, the peak at 0.9 V in Fig. 4a is also observed in Fig. 4d, albeit slightly shifted to 0.85 V. Given the absence of Ru(IV) species in the solution employed in the experiment of Fig. 4d, the peak at 0.85 V cannot be associated with tetramer oxidation as proposed by Maya. A further peak at ~1.2V is also seen in the CV of Fig. 4d which we shall return to below.

The peak at ~0.85 V was studied both as a function of voltage scan rate, Fig. 5a, and electrode rotation speed, Fig. 5b. The presence of both an oxidation and reduction peak in Fig. 5a suggests a broadly reversible process with a degree of quasi-/irreversibility as evidenced by the slight displacement in both the anodic and cathodic peak potentials with increasing scan rate. This modest irreversibility notwithstanding, the anodic peak currents show a square root dependence on scan rate, see Fig. 5a) indicating that it is associated with the oxidation of a solution, rather than surface adsorbed, species.

Current as a function of rotation speed data was recorded at a range of fixed potentials between the limits of 0.7 to 0.9 V i.e. in the vicinity of the anodic peak potential and in the region where mass transport control would be expected to dominate. As expected, currents were found to increase with rotation speed and Koutecky-Levich plots (28) of reciprocal current vs reciprocal square root of the rotation speed, are shown in Fig. 5b. According to the Randles-Sevcik and Koutecky-Levich equations, the slopes of the plots shown in Figs 5a. and 5b are given by eq. 2 and 3 respectively

$$\frac{d\ ip}{d\ \nu^{1/2}} = 0.4463.\frac{F^{3/2}}{RT^{1/2}}.A.C.D^{1/2}.n^{3/2} \qquad [2]$$

$$\frac{d\ 1/ip}{d\ 1/\omega^{1/2}} = \frac{1}{1.558.n.F.A.D^{2/3}C.\nu^{-1/6}} \qquad [3]$$

where i_p, ν, F, R, T, A, C, D, n and ω take their usual meanings. Eqs 2 and 3 exhibit different functional dependences on D and n, allowing for their evaluation if relevant slope values are available. Such slope values may be obtained from Figs. 5a and 5b, giving 2.00×10^{-5} and 28090 respectively (using the data recorded at 0.775 V in Fig 5b as this exhibits greatest linearity). Use of these slope values in accordance with eqs. 2 and 3 yielded values of n and D of 0.33 and 4×10^{-10} $m^2\ s^{-1}$ – the former being strong evidence for the peak at 0.85 V in Fig. 4d being associated with the oxidative formation from Ru(III) of a Ru(III)-Ru(IV)-Ru(III) trimer.

So as to further study the peak at 0.85 V, as well as the more anodic peak at ~1.2 V in Fig. 4d, a combined CV/voltamassogram was recorded from the same electroreductively pretreated solution of $RuCl_3$ over the slightly wider potential window of -0.4 to 2 V using carbon coated QCM crystals. Fig 5c shows the first scan recorded from such a crystal upon immersion in $RuCl_3$ solution, from which a number of observations may be made from the forward going scan.

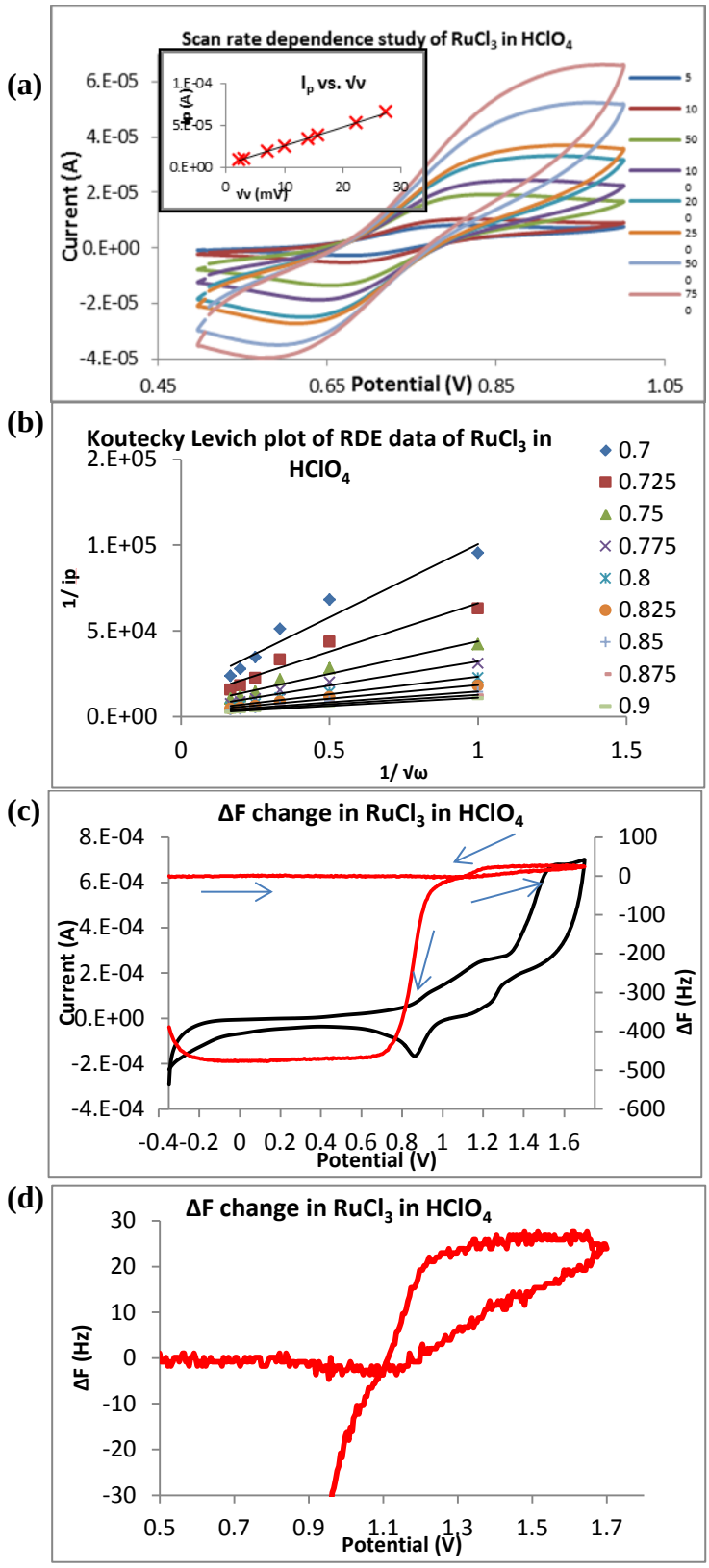

Figure 5 - a) Scan rate dependence study of electroreduced 10 mol dm^{-3} $RuCl_3$ in 0.1 mol dm^{-3} $HClO_4$. Legend shows scan rates in mV s^{-1}, Inset: I_P vs. √ν, b)Koutecky-Levich plots of RDE data from same solution every 25 mV from 0.7-0.9 V. ν = 1 mV s^{-1}, c) 1st scan cycle cyclic voltamassogram of same solution with the change in frequency of the crystal (red line), ν = 10 mV s^{-1} d) detail of frequency data from Figure 5c.

The first is that, as well as the peaks observed at 0.85 V and 1.2 V in the CV of Fig.4d, a third peak with a substantially higher peak current than either of the other two peaks is observed with an onset of ~1.3 V; this plateaus at ~1.7 V, just before the onset of a the displaced O_2 evolution wave on carbon. The second observation is that the peak at 0.85 V has no mass change associated with it in the voltamassogram trace, again suggesting that this peak is associated with a wholly solution phase process at the electrode surface, albeit one that results in the formation of an apparently soluble trimer species. The third observation is that the voltammetric peak at 1.2 V has a small mass increase associated with it whilst that at 1.3 V is associated with a similar, but opposite, mass loss.

Inspection of the Ru-H_2O E_h-pH diagram of Fig. 1 leads us to conclude that the mass increase at 1.2 V is due to RuO_2 formation at the carbon piezoelectrode surface. This is reversed almost immediately at 1.3 V as the so formed RuO_2 is converted to RuO_4, presumably evolved as a volatile gas. This latter assignment is supported by the fact that the peak current at 1.3 V is much larger than that at 0.85 V and 1.2 V – as might be expected if the peak at 1.3 V were associated with a 4 electron transfer Ru(IV) to Ru(VIII) transition compared to a 1 electron transfer Ru(III) to Ru(IV) reaction at 1.2 V and trimer formation with an average n value of 0.33 at 0.85 V. On the reverse scan, we see two mass gains at 1V and 0.8V. Upon consideration of the assignments in the forward going scan and the E_h-pH diagram of Figure 1, the former feature may be associated with on oxidation of Ru (III) to RuO_2, now giving rise to a mass increase due to the "switching off" of the following Ru(IV) to Ru(VIII) oxidation as the applied potential is decreased during the reverse scan); the latter feature is associated with the reduction of Ru (III) to Ru (0) metal at the piezoelectrode surface, giving rise to a resonant frequency decrease of the order of 500 Hz.

These reverse scan assignments are further supported by the second consecutive CVscan cycle using the same carbon-coated piezoelectrode and $RuCl_3$ solution as used to gather the data of Figures 5c and 5d. This second scan cycle is shown in Figure 6.

Both of the mass increases / resonant frequency decreases seen in the reverse scan of Figure 5c are seen in Figure 6 – first, a frequency decrease of ~100 Hz with a reverse scan

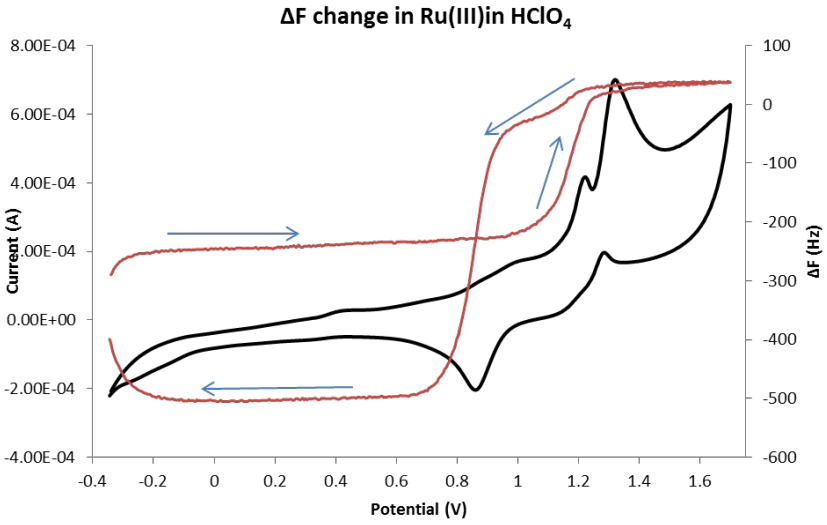

Figure 6 - 2nd scan cycle cyclic voltamassogram of same carbon coated piezoelectrode in the same 10 mol dm^{-3} $RuCl_3$ in 0.1 mol dm^{-3} $HClO_4$. solution used to record the data of Figures 5c and 5d. Voltammetric data is shown in black, microgravimetry data (expressed as a change in the frequency of the crystal) shown in red, ν = 10 mV s^{-1}.

onset of ~1.2 V and, second, a decrease of ~450 Hz with an onset of ~0.9 V. Both are associated with features in the corresponding reverse voltammetric trace – the decreases of 100 and 450 Hz with an oxidation peak at ~1.25 V and a reduction peak at ~0.9 V respectively. Again, Figure 1 indicates that features at 1.25 V are due to solution Ru(III) oxidation to solid RuO_2, whilst those at 0.9 V are due to reduction of Ru(III) to Ru metal.

However, both the forward going microgravimetric and voltammetric traces of Figure 6 exhibit differences to the corresponding traces of Figure 5c. The oxidation peaks at 1.2 V and E > 1.3 V are noticeably sharper in Figure 6 than in Figure 5c. The latter peak is still has no mass change associated with it and so, based on its size relative to adjacent peaks and the assignment of Figure 5c, can again be attributed to the oxidation of RuO_2 to RuO_4 – this happening almost immediately after the RuO_2 has been formed from solution phase Ru(III). In contrast, in Figure 6 the former peak at 1.2V is concurrent with a frequency increase / mass decrease of ~300 Hz that is not seen in Figure 5c. This can be explained by recalling that whilst the piezoelectrode presents a pristine carbon surface at the start of the first scan cycle, at the start of the second scan it is coated with a layer of metallic Ru deposited during the first scan – suggesting that the frequency increase / mass decrease of ~300 Hz is due to the oxidation of metallic Ru back to solution phase Ru(III) at 1.2 V, immediately prior to its further oxidation to volatile RuO_4 at E > 1.3 V.

It can be concluded therefore that the oxidation of solution phase Ru(III) to RuO_2 seen in the forward scan of Figure 5c occurs at a similar potential to the oxidation of Ru metal to Ru(III) in Figure 6. The Ru(III)/RuO_2 oxidation may very well be occurring at ~1.2 V in Figure 6; however, its associated current and mass change will be swamped by those associated with the Ru(0)/Ru(III) metal layer stripping process.

Conclusions

The electrochemistry of $RuCl_3$ in 0.1 mol dm^{-3} $HClO_4$ has been investigated using combined CV, RDE and electrochemical microgravimetry experiments for the first time. As purchased $RuCl_3$ was found to contain Ru in the +3/+4 oxidation states and so required exhaustive electroreduction to the +3 state before use. Using carbon electrodes due to their wider aqueous solvent window and lower faradaic interferences, four features have been identified in the forward going scan of the CV of $RuCl_3$ and two in the reverse.

The forward going features are: at ~0.8 V, an oxidation with no accompanying electrode mass change and a mean electron number of 0.33 suggesting the formation from solution phase Ru(III) of a solution phase Ru(III)-Ru(IV)-Ru(III) trimer; at ~1.2V during the first scan, an oxidation with an accompanying electrode mass increase, suggesting the deposition from Ru(III) solution phase species of solid RuO_2; also at ~1.2V in the second scan, during which the carbon surface will be coated with a Ru metal layer deposited during the first scan, an oxidation with an accompanying mass decrease due to the stripping of Ru metal to form solution phase Ru(III); and at E>1.3V, a large oxidation wave with little or no mass change associated with it which we assign to the almost immediate oxidation of the RuO2 generated at 1.2V to volatile RuO_4.

The reverse going features are: at ~1.2V, an oxidation with an accompanying electrode mass increase due to deposition of RuO_2 from Ru(III); and at ~0.9V a reduction peak with an accompanying large electrode mass increase which we assign to the reduction of solution phas Ru(III) to form Ru metal.

These assignments now provide insights into the baseline behaviour of Ru redox behaviour which the electrochemistry of NO complexed Ru species can be explored.

Acknowledgments

All data created during this research are openly available from Lancaster University data archive at http://dx.doi.org/10.17635/lancaster/researchdata/14. We thank the UK Engineering & Physical Sciences Research Council (iCASE Award No 11440238) Sellafield Sites Ltd (NNL Agreement 10009355) and the Lloyd's Register Foundation for financial support. Lloyd's Register Foundation supports the advancement of engineering-related education, and funds research and development that enhances safety of life at sea, on land and in the air.

References

1. Z. Holgye, M. Krivanek, *J. Radioanal.Chem*., **42**, 133 – 141 (1978).
2. T. Sato, *J. Radioanal.Chem.*, **129**, 77 - 84 (1989)
3. T. Sato, *J. Radioanal Chem.*,**139**, 25 - 29 (1990)
4. P. W. Cains, K. C. Yewer, S. Waring, *Radiochima. Acta.*, **56**, 99 – 104 (1992)
5. Y. Morris, A. Haig, *NNL Internal Communication*, 10, 10758, Issue 2 (2010)
6. Y. Morris, *NNL Internal Communication*, 10, 10750, Issue 2 (2010)
7. H. A. C. McKay, *BNFL Internal Report*, HAWGWP/P153 (1977)
8. P. W. Cains, AERE – R 9855 (1980)
9. D. Scargill, C.E. Lyon, N.R. Large, J.M. Fletcher, *J. Inorg. Nucl. Chem*., **27**, 161 - 171, (1965)
10. F. Mousset, F. Bedioui, C. Eysseric, *Elcetrochem. Comm*., **6**, 351 - 356 (2004)
11. P. Wehner,J. C. Hindman, *J. Amer. Chem. Soc*., **72**, 3911 - 3918 (1950)
12. L. W. Niedrach, A. D. Tevebaugh, *J. Amer. Chem. Soc*., **73**, 2835 - 2837 (1951)
13. D. K. Atwood, T. De Vries, *J. Amer. Chem. Soc*., **84**, 2659 - 2661 (1962)
14. L. Maya, *J. Inorg. Nucl. Chem*., **41**, 67 - 71 (1978)
15. R. M. Wallace, R. C. Propst, *J. Amer. Chem. Soc*., **91**, 3779 - 3785 (1969)
16. Y. Sugawara, A. P. Yadav, A. Nishikata, T. Tsuru, *J. Electrochem. Soc.,* **155**, B897 – B902 (2008)
17. L.D. Burke, D.T. Buckley, J.A. Morrissey, *Analyst*, **119** 841 - 845 (1994)
18. L.D. Burke, J.F. O'Sullivan, *Electrochim. Acta*, **37** 585 – 594 (1992)
19. L.D. Burke, B.H. Lee, *J. Electroanal. Chem*,. **330** 637 - 661 (1992)
20. S.G.D.Shackleford, C.Boxall, S.N.Port, R.J.Taylor, *J.Electroanal.Chem.*, **538-539**, 109-119 (2002)
21. A. J. Bard, R. Parsons, J. Jordan, *Standard Potentials in Aqueous Solution,* CRC Press, 1985
22. D.A. Buttry, *Electroanal. Chem.*, **17**, 1 - 85 (1991)
23. D.A. Buttry, *Electrochemical Interfaces: Modern Techniques for In-Situ Interface Characterisation*, H.D. Abruna, Editor, VHC Publishers Inc., 529-566, (1991)
24. M.R. Deakin, D.A. Buttry, *Anal. Chem*., **61**, 1147A-1154A, (2008)
25. C. Gabrielli, M. Keddam, R. Torresi, *J. Electrochem. Soc*. **138(9)**, 2657-2660 (1991)
26. G. L. Borges, K. K. Kanazawa, J. G. Gordan II, *J. Electroanal. Chem*. **364(1-2)**, 281-284 (1994)
27. X. Yan, H. Liu, K. W. Liew, *J. Mat. Chem.*, **11**, 3387 - 3391 (2001)
28. A. J. Bard, L. R. Faulkner, *Electrochemical Methods: Fundamentals and Applications,* John Wiley & Sons, Inc., (2001)